


## PREPARATION OF ALLANTOIN LOADED CHITOSAN NANOPARTICLES AND INFLUENCE OF MOLECULAR WEIGHT OF CHITOSAN ON DRUG RELEASE

### Allantoin Yüklü Kitosan Nanopartiküllerinin Hazırlanması ve Kitosanın Moleküler Ağırlığının İlaç Salımı Üzerindeki Etkisi

Ahmet ULU<sup>1</sup> 

<sup>1</sup>Inonu University, Faculty of Arts and Science, Malatya, Turkey

Geliş Tarihi / Received: 29.06.2020

Kabul Tarihi / Accepted: 07.10.2020

Yayın Tarihi / Published: 30.11.2020

#### ABSTRACT

In this study, allantoin-loaded chitosan nanoparticles were prepared and the effect of molecular weights (low, medium, and high) of chitosan was investigated on the release of allantoin. The allantoin-loaded chitosan nanoparticles were characterized by various methods. The morphology, size, zeta potential, and loading efficiency were affected by the molecular weight of chitosan. The results displayed that the average hydrodynamic diameter of chitosan nanoparticles was in the range of 427–768 nm and the zeta potential values from 5.97 to 5.12 mV was obtained. The allantoin release from chitosan nanoparticles reached the plateau level in 96 hours. Cumulative allantoin release values of low, medium, and high molecular mass chitosan nanoparticles were determined as 43%, 30%, and 27%, respectively. According to the results, the molecular weight of chitosan influenced on allantoin release.

**Keywords:** Allantoin, Chitosan Nanoparticles, Drug Release, Molecular Weights

#### ÖZ

Bu çalışmada, allantoin yüklü kitosan nanopartikülleri hazırlanmış ve kitosanın moleküler ağırlıklarının (düşük, orta ve yüksek) allantoin salınımı üzerindeki etkisi araştırılmıştır. Allantoin yüklü kitosan nanopartikülleri çeşitli yöntemlerle karakterize edilmiştir. Morfoloji, boyut, zeta potansiyeli ve yükleme etkinliği, kitosanın moleküler ağırlığından etkilenmiştir. Sonuçlar, kitosan nanopartiküllerinin ortalama hidrodinamik çapının 427-768 nm aralığında olduğunu ve 5.97 ila 5.12 mV'lik zeta potansiyelinin elde edildiğini göstermiştir. Kitosan nanopartiküllerinden allantoin salınımı 96 saat içinde plato seviyesine ulaşmıştır. Kümülatif allantoin salım değerleri düşük, orta ve yüksek molekül ağırlıklı kitosan nanopartikülleri için sırasıyla %43, %30 ve % 27 olarak tespit edilmiştir. Sonuçlara göre kitosanın molekül ağırlığı allantoin salınımını etkilemiştir.

**Anahtar kelimeler:** Allantoin, İlaç Salınımı, Kitosan Nanopartiküller, Moleküler Ağırlığı

---

## INTRODUCTION

In recent years, natural and synthetic polymeric materials have been extensively utilized as a drug carrier in drug delivery applications (Odeniyi, Omoteso, Adepoju, & Jaiyeoba, 2018; Severino et al., 2019). Among them, chitosan (CHS) has a promising carrier because it has many superior properties, such as nontoxicity, biocompatibility, and biodegradability (Meng, Zhang, Agrahari, Ezoulin, & Youan, 2014). It is a water-soluble, linear cationic polysaccharide, that is obtained by the deacetylation of chitin, which is one of the most abundant natural polysaccharides (Meng, Sturgis, & Youan, 2011). Moreover, CHS has functional groups, such as hydroxyl, amine, and amide groups (Senda, He, & Inoue, 2002). Therefore, it can be easily modified and interacted with other compounds for various applications. In particular, free amino groups of CHS can be positively charged in an acidic environment, which allows interaction with the negatively charged compound for drug delivery applications (Calvo, Remuñan-López, Vila-Jato, & Alonso, 1997; Meng et al., 2011). Sodium tripolyphosphate (STPP) is a polyvalent anion with three negatively charged phosphate groups. Therefore, it can be crosslinked with CHS. Chitosan nanoparticles (CHS NPs) occur spontaneously with intermolecular and molecular bonds formed between the amino groups of CHS and the phosphate of STPP (Calvo et al., 1997; Meng et al., 2011). CHS NPs have been commonly used because of favorable advantages such as biodegradability, ease of synthesis, biocompatibility, and low cost for drug delivery applications (Cetin et al., 2007; Naskar, Koutsu, & Sharma, 2019; Tiğli Aydın & Pulat, 2012).

The allantoin (5-ureide-hydantoin) is a natural active compound that helps to alleviate skin irritation and moisturize the skin by regulating the anti-inflammatory response, stimulating extracellular matrix synthesis and fibroblast proliferation (Yaşayan, Karaca, Akgüner, & Bal Öztürk, 2020). It is widely used in cosmetic and pharmaceutical preparations for different therapeutic purposes (Araújo, Grabe-Guimarães, Mosqueira, Carneiro, & Silva-Barcellos, 2010). However, there are very few studies reporting allantoin release in literature. For example, Ke et al. (Ke et al., 2016) prepared, characterized, and investigated the allantoin release properties of allantoin-loaded porous silica nanoparticles/polycaprolactone nanofiber composites. In another study, Yaşayan et al. (Yaşayan et al., 2020) fabricated chitosan/collagen composite films encapsulating allantoin and lidocaine hydrochloride as wound dressing material.

To the best of my knowledge, this is the first article to investigate the use of CHS NPs in allantoin release. For this purpose, we prepared chitosan nanoparticles (CHS NPs) from

CHS of different molecular weights via ionic gelation, and the effect of CHS molecular weight was investigated on the release of allantoin. The physicochemical characteristics of CHS NPs such as functional group, crystallinity, particle size, zeta potential, morphology, elemental analysis was evaluated by using Fourier transform infrared spectroscopy-attenuated total reflectance (FTIR-ATR), X-ray diffraction (XRD), dynamic light scattering (DLS), scanning electron microscopy (SEM), energy-dispersive X-ray spectroscopy (EDX). In addition, loading efficiency and the *in vitro* release profile of allantoin was evaluated at pH=5.

## **MATERIALS AND METHODS**

### **Materials**

Low-molecular weight CHS (75-85% deacetylated), medium-molecular weight CHS (75-85% deacetylated), high-molecular weight CHS (>75% deacetylated), glacial acetic acid, allantoin ( $\geq 98\%$ ) were purchased from Sigma-Aldrich. Sodium triphosphate (STPP) was obtained from Merck. All other chemicals were reagent grade and used without further purifications. The ultrapure water was used in all experiments.

### **Preparation of CHS NPs**

The CHS NPs were prepared by using the ionic interaction between positively charged CHS solution and negatively charged STPP solution (Figure 1) (Li, Wang, Peng, She, & Kong, 2011; Rampino, Borgogna, Blasi, Bellich, & Cesàro, 2013). Briefly, the CHS powders were firstly dissolved in 1% aqueous acetic acid solution at a concentration of 3 mg ml<sup>-1</sup>. The CHS solutions were stirred overnight to obtain a homogeneous and clear solution. The pH value of the CHS solution was adjusted to 5.5 using NaOH aqueous solution (1 M). Meanwhile, STPP powder was dissolved in distilled water with a concentration of 2 mg ml<sup>-1</sup> and filtered through 0.45  $\mu$ m membrane filter. Afterward, 4 ml of the STPP solution was dropped into 10 ml of the CHS solutions under vigorous magnetic stirring at room temperature. The resulting mixture was kept stirring for 30 min to complete ionic gelling and to form CHS NPs. After 30 min, the formed CHS NPs were collected by centrifugation at 14.000 rpm for 30 min. To calculate loading efficiency, the supernatants were kept at room temperature. Finally, the collected CHS NPs were lyophilized for 24 h by using a freeze dryer under -80 °C and stored at +4 °C for next use.

### **Preparation of the allantoin-loaded CHS NPs**

The allantoin-loaded CHS NPs were synthesized in the same way as described for CHS NPs. Allantoin ( $1.5 \text{ mg ml}^{-1}$ ) was dissolved directly in STPP solution before the preparation of CHS NPs and the above method was then applied.

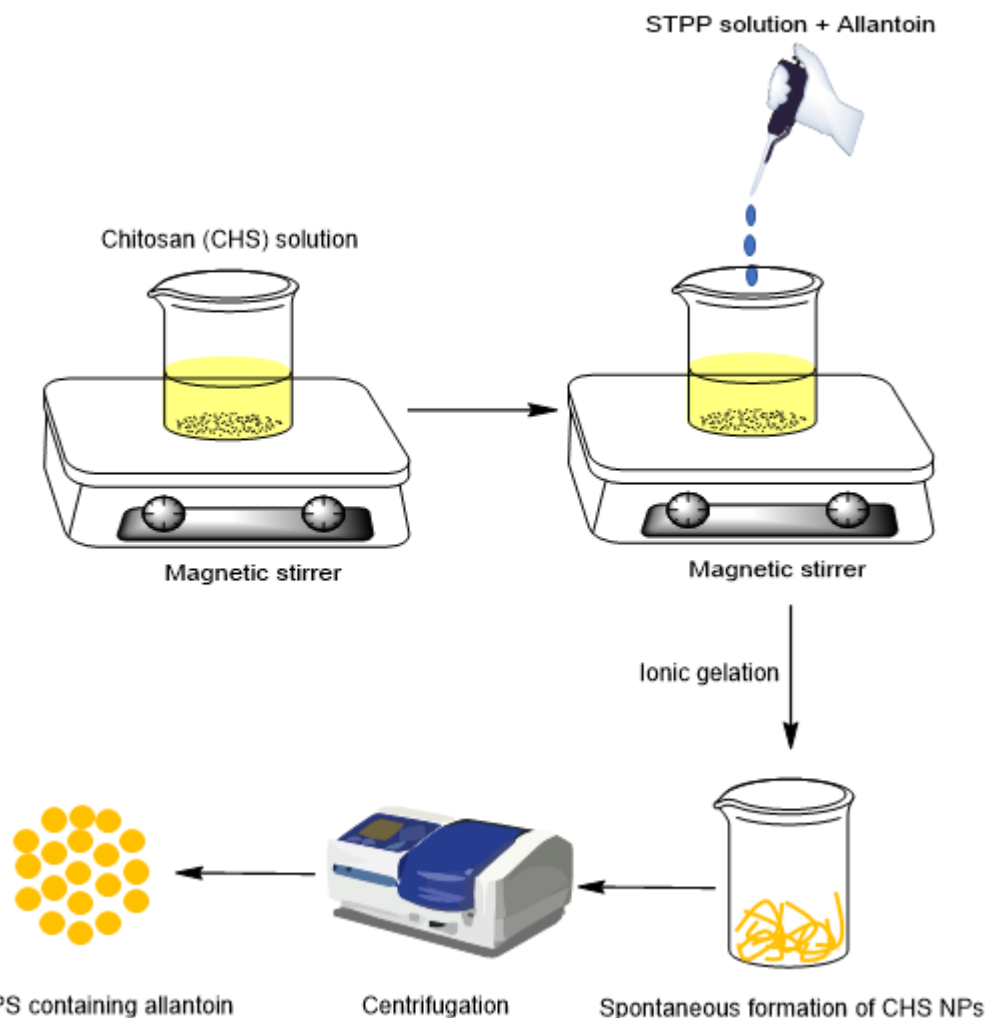


**Figure 1.** Schematic Diagram of Preparation of the Allantoin-Loaded and Pure CHS NPs.

## Characterization methods

### FTIR-ATR analysis

The FTIR-ATR spectra of samples were determined using an FTIR-ATR (PerkinElmer). The spectra were recorded in the region between  $4000$  and  $400 \text{ cm}^{-1}$ .

### XRD analysis

XRD patterns of CHS NPs crosslinking with STPP were obtained by using powder XRD (Rigaku RadB). The CHS NPs were analyzed in  $2\theta$  angle range of  $2\text{--}80^\circ$  at a scanning rate of  $2^\circ 2\theta^{-1} \text{ min}^{-1}$ .

### Hydrodynamic diameter and zeta potential measurement

Average hydrodynamic diameter and zeta potential values of the prepared NPs were measured by using a Zetasizer Nano ZS (Malvern, UK). Size measurements were carried out at room temperature.

### **SEM and EDX analysis**

The micrographs of all samples were analyzed by SEM (LEO Evo-40 VPX). EDX analysis was carried out via a Rontec Xflash detector analyzer equipped with SEM.

### **Loading efficiency (LE)**

Allantoin-loaded CHS NPs were separated from the suspension by centrifugation at 10.000 rpm for 30 minutes. The supernatant was collected and was assayed by UV spectrophotometer (UV-1601 Shimadzu) at 230 nm. The LE value was calculated using the following formula:

$$LE (\%) = \frac{\text{Total allantoin} - \text{Free allantoin}}{\text{Total allantoin}} \times 100$$

### ***In vitro* release of allantoin**

The *in vitro* drug release of allantoin from CHS nanoparticles was investigated via the dialysis tubing membrane technique. Briefly, the freeze-dried CHS-allantoin nanoparticles (20 mg) were placed into dialysis tubes. The dialysis tubes were soaked into PBS solutions (pH: 5.0) and were incubated at 37 °C under gent magnetic stirring. At determined time intervals, 1 ml of the release media was taken and was replaced with an equivalent volume of fresh PBS solution to keep the volume of the system identical. The cumulative release of allantoin was determined by using a UV-Vis spectrophotometer (Shimadzu, 1601) at 230 nm (Becker et al., 2010). The released allantoin concentration was then calculated using the previously prepared standard allantoin calibration curve.

## **RESULTS AND DISCUSSION**

### **FTIR-ATR analysis**

FTIR spectra of the prepared CHS NPs are shown in Figure 2. As expected, similar peaks were observed in all spectra. For instance, the peak at 3200-3600 cm<sup>-1</sup> stem from H-bond stretching vibration of -NH<sub>2</sub> and -OH groups. The peaks at 1638 cm<sup>-1</sup>, 1540 cm<sup>-1</sup>, and 1317 cm<sup>-1</sup> are due to the C=O stretching (amide I), N-H bending (amide II) and C-N stretching (amide III), respectively. In addition, the absorption peaks at 1057 cm<sup>-1</sup> and 870 cm<sup>-1</sup> are the presence of the anti-symmetric stretching vibration of C-O-C bridges and

glucopyranose ring of CHS. Similar FTIR results for CHS NPs were reported in previous works (Lustriane, Dwivany, Suendo, & Reza, 2018; Mohammadpour Dounighi et al., 2012; OH, Chun, & Chandrasekaran, 2019).

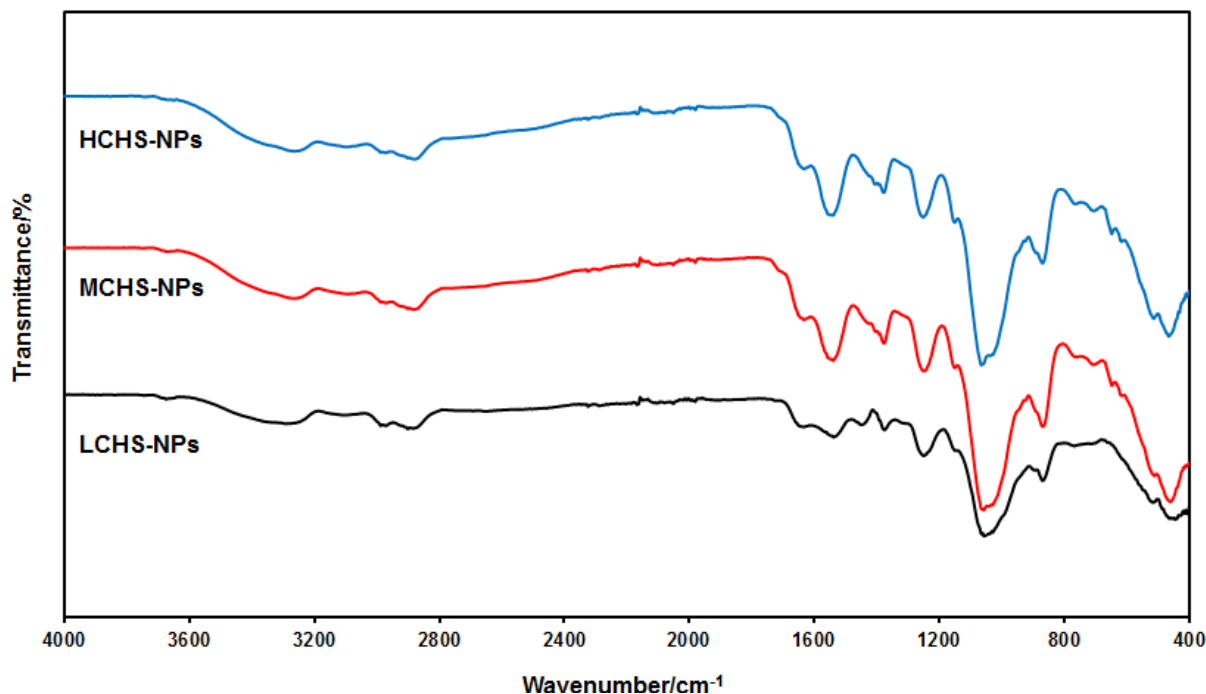


**Figure 2.** The FTIR Spectra of the Prepared LCHS-NPs, MCHS-NPs, and HCHS-NPs.

### XRD analysis

Figure 3 presents XRD patterns of LCHS, MCHS, HCHS, LCHS-NPs, MCHS-NPs and HCHS-NPs. The XRD patterns of the samples are similar to each other. From the patterns, the two main peaks were appeared at  $2\theta = 10^\circ$  and  $20^\circ$ . Even though CHS has a semi crystalline structure, this behavior reduces because of the breaking of hydrogen bonds when it is cross-linked with STPP (Fan, Yi, Zhang, & Yokoyama, 2017). These results correspond well with the XRD patterns reported by Villegas-Peralta et al. (Villegas-Peralta et al., 2020).

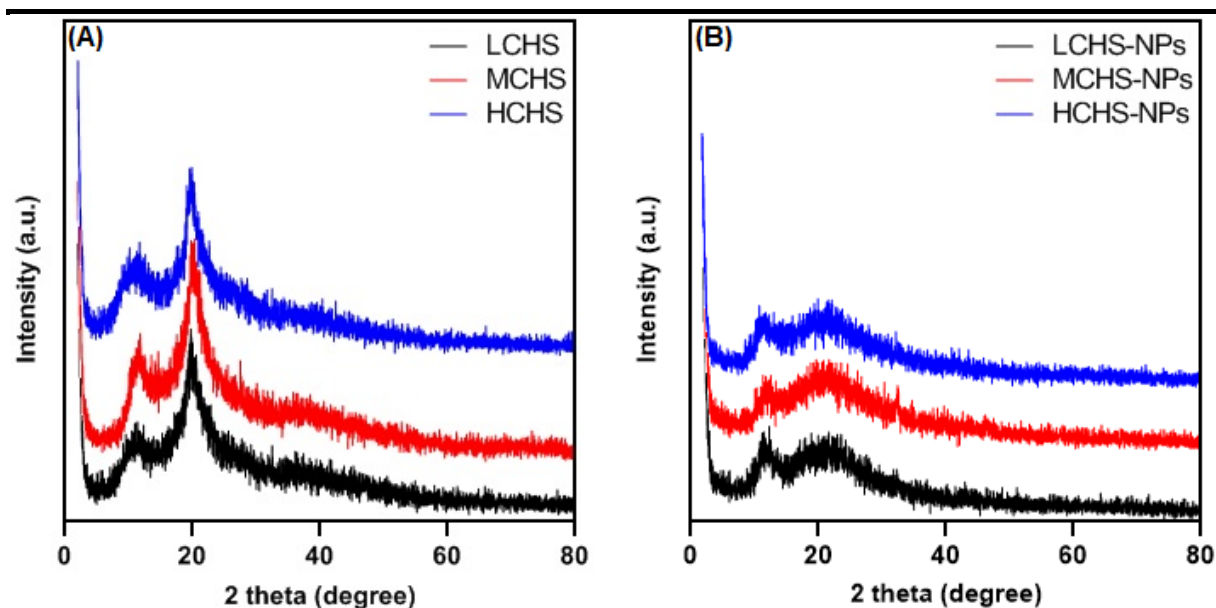


**Figure 3.** The XRD Patterns of (A) LCHS, MCHS, and HCHS, (B) the Prepared LCHS-NPs, MCHS-NPs, and HCHS-NPs.

### Hydrodynamic diameter and zeta potential measurement

DLS was used to evaluate the average hydrodynamic diameter of CHS NPs and the measured results were demonstrated in Table 1. As the molecular weight of CHS increases, size of the CHS NPs increased. The average diameters for the prepared LCHS-NPs, MCHS-NPs and HCHS-NPs were found to be  $427\pm 43.8$ ,  $663\pm 68.5$ , and  $768\pm 79.1$  nm, respectively. High hydrodynamic diameter values obtained from DLS are the result of the particle aggregation. A similar phenomenon was reported by Taghizadeh & Bahadori (Taghizadeh & Bahadori, 2013). They claimed that the hydrodynamic diameter depends on degree of substitution and deacetylation degree of CHS since CHS NPs are prepared by the ionic crosslinking between positive charged ammonium ions of CHS and negative ions of STPP. In addition, Desai et al. (Desai & Park, 2005; Desai, Liu, & Park, 2006) reported that the viscosity of the polymer solution increases with an increase in its molecular weight. Thus, droplets formed from a higher viscosity and molecular weight CHS solution become larger, resulting in larger-sized particles.

Additionally, the zeta potential values of the prepared LCHS-NPs, MCHS-NPs and HCHS-NPs were  $+5.97\pm 0.96$  mV,  $+5.30\pm 0.20$  mV, and  $+5.12\pm 0.38$ , respectively. The lowest zeta potential value was obtained for HCHS-NPs, which due to agglomerates. In a similar study, Villegas-Peralta et al. (Villegas-Peralta et al., 2020) reported that when molecular weight in CHS increases, a reduction in the zeta potential was observed.

**Table 1.** The Average Hydrodynamic Diameter and Zeta Potential Values of the Prepared LCHS-NPs, MCHS-NPs, and HCHS-NPs.

Sample code	Hydrodynamic diameter (nm)	Zeta potential (mV)
LCHS-NPs	427±43.8	+5.97±0.96
MCHS-NPs	663±68.5	+5.30±0.20
HCHS-NPs	768±79.1	+5.12±0.38

### SEM and EDX analysis

The surface morphology of the CHS NPs was investigated by SEM. Figure 4 indicates the SEM micrographs at 20.00 KX magnification of the prepared CHS NPs. It can be observed that all SEM micrographs displayed rough and porous structure due to rapid agglomeration caused by hydrogen bonds (Uppal et al., 2018; Villegas-Peralta et al., 2020). Besides, the CHS NPs showed a bigger particle size. These results were in agreement with previous studies (Feyzioglu & Tornuk, 2016; Kahdestani, Shahriari, & Abdouss, 2020). Finally, the difference in surface morphology of the CHS NPs obtained from the SEM image almost negligible.



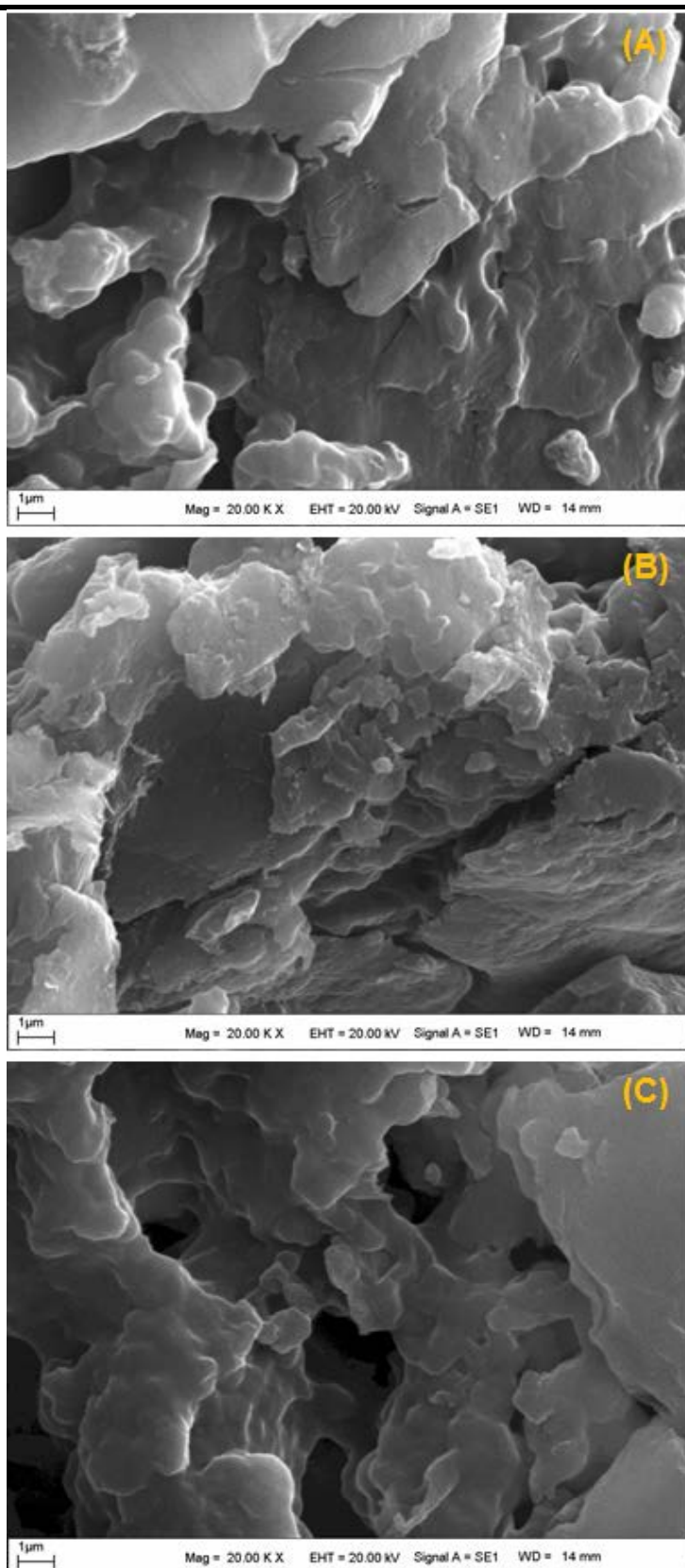


**Figure 4.** The SEM Micrographs at 20.00 KX Magnification of the Prepared LCHS-NPs (A), MCHS-NPs (B), and HCHS-NPs (C).

The elemental composition of the prepared CHS NPs was investigated by using the EDX analysis (Figure 5). As can be seen, while carbon (C), oxygen (O), and nitrogen (N)

peaks were seen in all EDX patterns due to chitosan, the presence of sodium (Na) and phosphorus (P) verified the formation of CHS nanoparticles cross-linked with STPP (Villegas-Peralta et al., 2020). As expected, as the molecular weight of chitosan increased, the peak intensity of the C, N, and O elements increased. Unlike, the amounts of phosphorus for CHS NPs were very similar. These findings paralleled with those reported by Villegas-Peralta et al. (Villegas-Peralta et al., 2020).

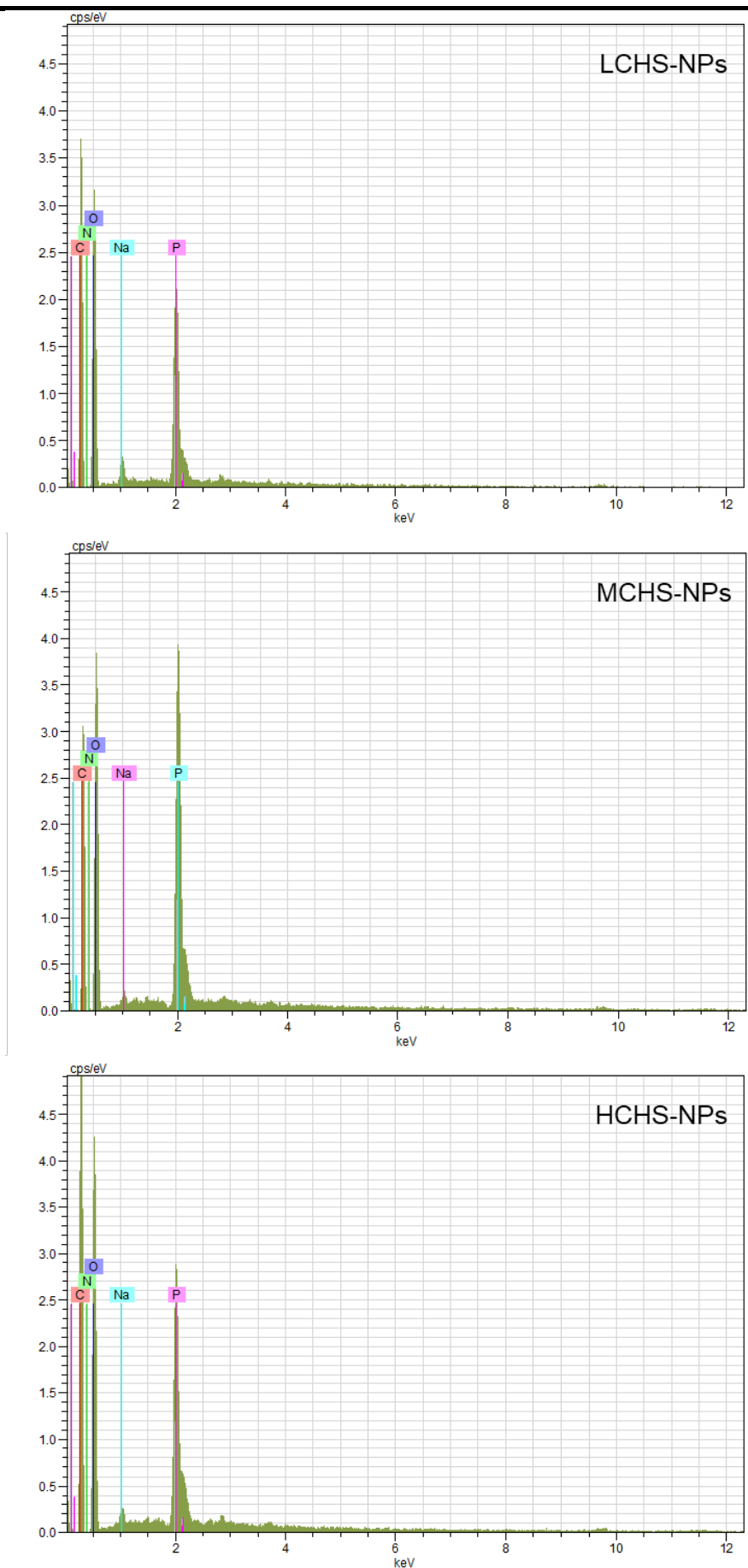


**Figure 5.** The EDX Patterns of the Prepared LCHS-NPs, MCHS-NPs, and HCHS-NPs.

The EDX-mapping images shown in Figure 6 also confirm previous characterization results.

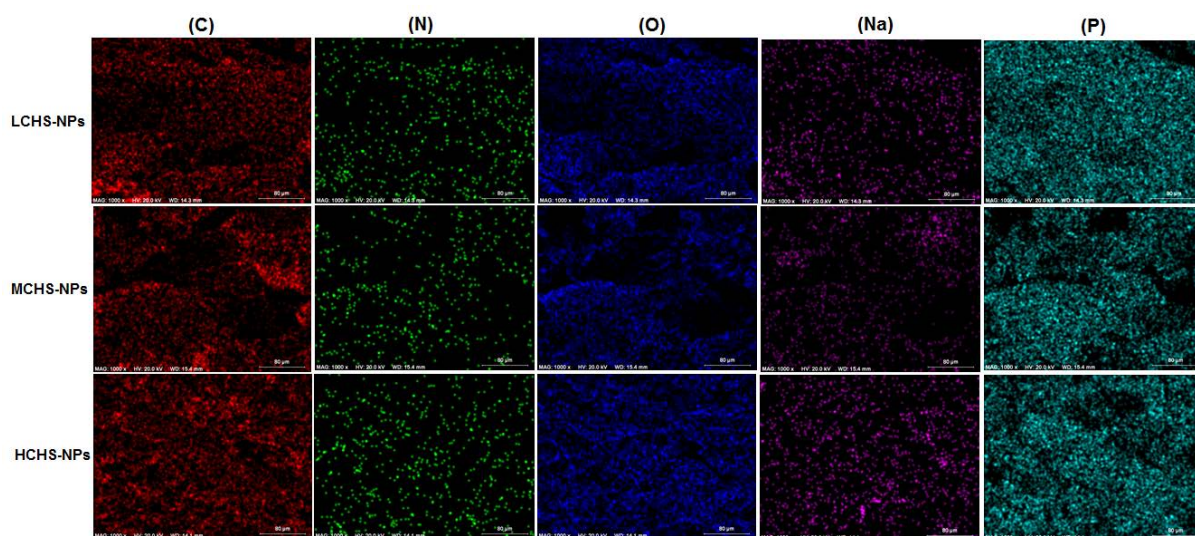


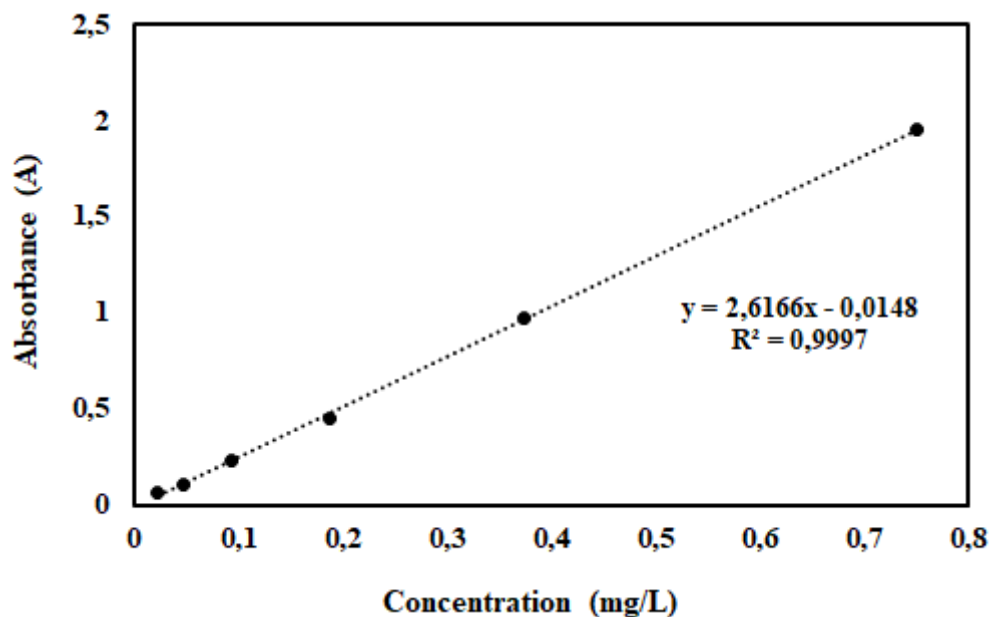
**Figure 6.** The EDX-Mapping Images of Elements in the Prepared LCHS-NPs, MCHS-NPs, and HCHS-NPs.

### **Loading efficiency**

The LE values of allantoin into CHS NPs was 52.10%, 51.28%, and 41.80% for LCHS-NPs, MCHS-NPs, and HCHS-NPs, respectively. The loading efficiency did not change significantly for LCHS-NPs, MCHS-NPs, however, it decreased when allantoin was encapsulated into HCHS-NPs. Most probably, the low molecular weight of the CHS solution containing the shorter CHS chains made its free amino groups easier to protonate and, thus, led to higher encapsulation of allantoin via ionic interactions (Yang & Hon, 2009). Therefore, loading efficiency reduced with an increase in the molecular weight of CHS. These results are parallel with the previous reports. (Desai et al., 2006; Filipović-Grčić et al., 2003)

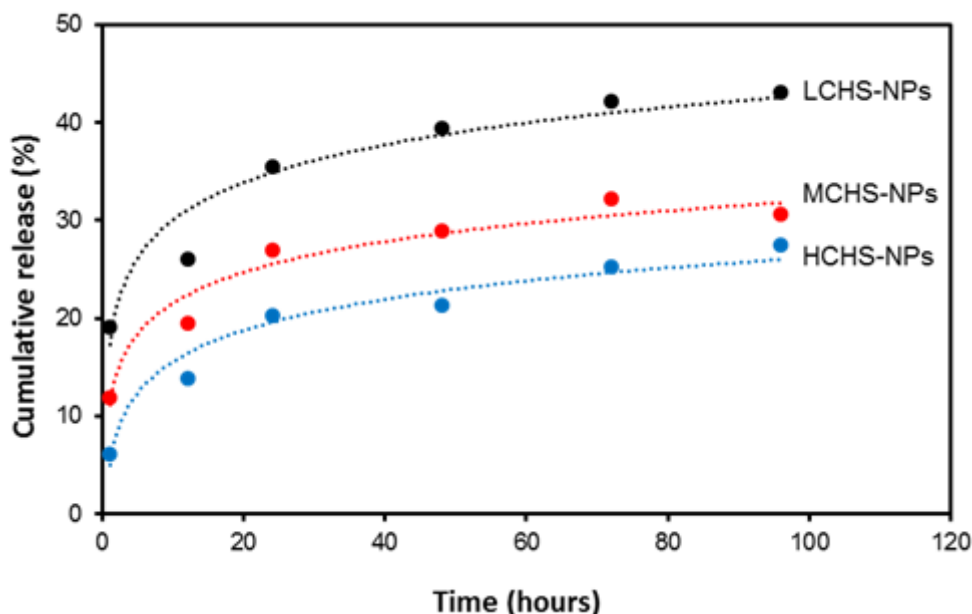
### ***In vitro* release of allantoin**

Figure 7 presents the calibration graph used to determine the amounts of allantoin released from the CHS NPs.



**Figure 7.** Calibration Curve of Allantoin.

The results of the effect of the molecular weight of CHS on the allantoin release from the CHS NPs are shown in Figure 8. The molecular weight of CHS remarkably influenced the allantoin release from CHS NPs. Interestingly, allantoin was quickly released from the CHS NPs in 12 hours, and then its release was slower. For instance, after 24 hours, the allantoin released reached 39.44%, 28.88%, and 21.38% for LCHS-NPs, MCHS-NPs, and HCHS-NPs, respectively. After 96 hours, these values reached the plateau level recorded as 43.11%, 30.66%, and 27.55, respectively. The reason allantoin releases from the LCHS-NPs more quickly than from the MCHS-NPs, and HCHS-NPs might be because of the smaller particle size. Because of the smaller particle size, the nanoparticles can dissolve and diffuse into the buffer solution more easily, releasing allantoin from CHS NPs faster (Thai et al., 2020).



**Figure 8.** The Release Profile of Allantoin Loaded CHS NPs.

## CONCLUSIONS

The scope of the current work was to encapsulate allantoin into CHS NPs and to examine the effect of the molecular weight of CHS on *in vitro* release of allantoin. Allantoin-loaded chitosan nanoparticles were successfully produced by using ionic gelation, as characterized by instrumental analytical techniques including FTIR, XRD, DLS, SEM, and EDX. According to DLS results, although the hydrodynamic diameter of chitosan nanoparticles increased with increasing the molecular weight of chitosan, zeta potential values decreased. In addition, by increasing the molecular weight of CHS, the LE value decreased. The *in vitro* release results revealed that the molecular weight of CHS influenced the release rate of allantoin from the CHS NPs. The results suggested that the CHS NPs might be used as a carrier for allantoin.

## ACKNOWLEDGEMENTS

The author thanks Prof. Dr. Burhan Ateş.

## Conflict of interests

The author declares that there is no conflict of interest with any person, institute, company, etc.

## REFERENCES

Araújo, L. U., Grabe-Guimarães, A., Mosqueira, V. C. F., Carneiro, C. M., Silva-Barcellos, N. M. (2010). Profile of wound healing process induced by allantoin1. *Acta Cirurgica Brasileira*, 25(5), 460–466.

- Becker, L. C., Bergfeld, W. F., Belsito, D. V., Klaassen, C. D., Marks Jr, J. G., Shank, R. C., ... Andersen, F. A. (2010). *Final report of the safety assessment of allantoin and its related complexes. International Journal of Toxicology*, 29(2), 84-97.
- Calvo, P., Remuñan-López, C., Vila-Jato, J. L., Alonso, M. J. (1997). *Chitosan and chitosan/ethylene oxide-propylene oxide block copolymer nanoparticles as novel carriers for proteins and vaccines. Pharmaceutical Research*, 14(10), 1431-1436.
- Cetin, M., Aktas, Y., Vural, I., Capan, Y., Dogan, L. A., Duman, M., ... Dalkara, T. (2007). *Preparation and in vitro evaluation of bFGF-loaded chitosan nanoparticles. Drug Delivery*, 14(8), 525-529.
- Desai, K. G. H., Park, H. J. (2005). *Encapsulation of vitamin C in tripolyphosphate cross-linked chitosan microspheres by spray drying. Journal of Microencapsulation*, 22(2), 179-192.
- Desai, K. G., Liu, C., Park, H. J. (2006). *Characteristics of vitamin C encapsulated tripolyphosphate-chitosan microspheres as affected by chitosan molecular weight. Journal of Microencapsulation*, 23(1), 79-90.
- Fan, Y., Yi, J., Zhang, Y., Yokoyama, W. (2017). *Improved chemical stability and antiproliferative activities of curcumin-loaded nanoparticles with a chitosan chlorogenic acid conjugate. Journal of Agricultural and Food Chemistry*, 65(49), 10812-10819.
- Feyzioglu, G. C., Tornuk, F. (2016). *Development of chitosan nanoparticles loaded with summer savory (Satureja hortensis L.) essential oil for antimicrobial and antioxidant delivery applications. LWT - Food Science and Technology*, 70, 104-110.
- Filipović-Grčić, J., Perissutti, B., Moneghini, M., Voinovich, D., Martinac, A., Jalšenjak, I. (2003). *Spray-dried carbamazepine-loaded chitosan and HPMC microspheres: preparation and characterisation. Journal of Pharmacy and Pharmacology*, 55(7), 921-931.
- Kahdestani, S. A., Shahriari, M. H., Abdouss, M. (2020). *Synthesis and characterization of chitosan nanoparticles containing teicoplanin using sol-gel. Polymer Bulletin*, 1-16.
- Ke, M., Wahab, J. A., Hyunsik, B., Song, K. H., Lee, J. S., Gopiraman, M., ... Kim, I. S. (2016). *Allantoin-loaded porous silica nanoparticles/ polycaprolactone nanofiber composites: fabrication, characterization, and drug release properties. RSC Advances*, 6, 4593-4600.
- Li, P., Wang, Y., Peng, Z., She, F., Kong, L. (2011). *Development of chitosan nanoparticles as drug delivery systems for 5-fluorouracil and leucovorin blends. Carbohydrate Polymers*, 85(3), 698-704.
- Lustriane, C., Dwivany, F. M., Suendo, V., Reza, M. (2018). *Effect of chitosan and chitosan-nanoparticles on post harvest quality of banana fruits. Journal of Plant Biotechnology*, 45(1), 36-44.
- Odeniyi, M. A., Omotoso, O. A., Adepoju, A. O., Jaiyeoba, K. T. (2018). *Starch nanoparticles in drug delivery: a review. Polimery w Medycynie*, 48(1), 41-45.
- Meng, J., Sturgis, T. F., Youan, B. B. C. (2011). *Engineering tenofovir loaded chitosan nanoparticles to maximize microbicide mucoadhesion. European Journal of Pharmaceutical Sciences*. 44(1-2):57-67.
- Meng, J., Zhang, T., Agrahari, V., Ezoulin, M. J., Youan, B. B. C. (2014). *Comparative biophysical properties of tenofovir-loaded, thiolated and nonthiolated chitosan nanoparticles intended for HIV prevention. Nanomedicine*, 9(11), 1595-1612.
- Mohammadpour Dounighi, N., Eskandari, R., Avadi, M. R., Zolfagharian, H., Mir Mohammad Sadeghi, A., & Rezayat, M. (2012). *Preparation and in vitro characterization of chitosan nanoparticles containing Mesobuthus eupeus scorpion venom as an antigen delivery system. Journal of Venomous Animals and Toxins Including Tropical Diseases*. 18(1), 44-52.
- Naskar, S., Koutsu, K., Sharma, S. (2019, April 21). *Chitosan-based nanoparticles as drug delivery systems: a review on two decades of research. Journal of Drug Targeting*. 27, 379-393.

- 
- OH, J.-W., Chun, S. C., Chandrasekaran, M. (2019). Preparation and in vitro characterization of chitosan nanoparticles and their broad-spectrum antifungal action compared to antibacterial activities against phytopathogens of tomato. *Agronomy*, 9(1), 21.
- Rampino, A., Borgogna, M., Blasi, P., Bellich, B., Cesàro, A. (2013). Chitosan nanoparticles: Preparation, size evolution and stability. *International Journal of Pharmaceutics*, 455(1–2), 219–228.
- Senda, T., He, Y., Inoue, Y. (2002). Biodegradable blends of poly( $\epsilon$ -caprolactone) with  $\alpha$ -chitin and chitosan: specific interactions, thermal properties and crystallization behavior. *Polymer International*, 51(1), 33–39.
- Severino, P., da Silva, C. F., Andrade, L. N., de Lima Oliveira, D., Campos, J., Souto, E. B. (2019). Alginate nanoparticles for drug delivery and targeting. *Current Pharmaceutical Design*, 25(11), 1312–1334.
- Taghizadeh, M. T., Bahadori, A. (2013). Preparation, characterization and adhesive properties of di- and tri-hydroxy benzoyl chitosan nanoparticles. *Chinese Journal of Polymer Science*, 31(4), 649–659.
- Thai, H., Thuy Nguyen, C., Thi Thach, L., Thi Tran, M., Duc Mai, H., Thi Thu Nguyen, T., ... Van Le, Q. (2020). Characterization of chitosan/alginate/lovastatin nanoparticles and investigation of their toxic effects in vitro and in vivo. *Scientific Reports*, 10(1), 909.
- Tiğli Aydın, R. S., Pulat, M. (2012). 5-fluorouracil encapsulated chitosan nanoparticles for pH-stimulated drug delivery: Evaluation of controlled release kinetics. *Journal of Nanomaterials*, 313961.
- Uppal, S., Kaur, K., Kumar, R., Kaur, N. D., Shukla, G., Mehta, S. K. (2018). Chitosan nanoparticles as a biocompatible and efficient nanowagon for benzyl isothiocyanate. *International Journal of Biological Macromolecules*, 115, 18–28.
- Villegas-Peralta, Y., López-Cervantes, J., Madera Santana, T. J., Sánchez-Duarte, R. G., Sánchez-Machado, D. I., Martínez-Macías, M. del R., Correa-Murrieta, M. A. (2020). Impact of the molecular weight on the size of chitosan nanoparticles: characterization and its solid-state application. *Polymer Bulletin*, 1-20.
- Yang, H. C., Hon, M. H. (2009). The effect of the molecular weight of chitosan nanoparticles and its application on drug delivery. *Microchemical Journal*, 92(1), 87–91.
- Yaşayan, G., Karaca, G., Akgüner, Z. P., Bal Öztürk, A. (2020). Chitosan/collagen composite films as wound dressings encapsulating allantoin and lidocaine hydrochloride. *International Journal of Polymeric Materials and Polymeric Biomaterials*, 1-13.